BIBECHANA
Vol. 20, No. 1, April 2023, 55-64

ISSN 2091-0762 (Print), 2382-5340 (Online)
Journal homepage: http://nepjol.info/index.php/BIBECHANA
Publisher:Dept. of Phys., Mahendra Morang A. M. Campus (Tribhuvan University)Biratnagar

Analysis and characterization of X-ray flare of Mkn 421 using *XMM-Newton* observation 0658801301

Rajendra Neupane, Niraj Dhital*

Central Department of Physics, Tribhuvan University, Nepal

*Corresponding author. Email: niraj.dhital@cdp.tu.edu.np

Abstract

This research work was carried out to analyze the X-ray flares in Blazar Mkn 421 using data from XMM-Newton observation (Observation ID: 0658801301) that lasted for 8 hours. EPIC/pn data was used for statistical analysis of the light and spectrum curve in energy ranges from 0.3 to 10.0 keV. The best fit model for the spectrum was found to be the additive model (log-parabola + black-body). The measured integrated flux in the energy range of 0.3-2 keV is 5.015 × 10^{-10} ergs cm^{-2} s^{-1} with an associated uncertainty range of (5.010 – 5.020) × 10^{-10} ergs cm^{-2} s^{-1} at a 90% confidence level. Similarly, the measured integrated flux in the energy range of 2-10 keV is 2.398 × 10^{-10} ergs $cm^{-2}s^{-1}$ with an associated uncertainty range of (2.392 – 2.405) × 10^{-10}ergs cm^{-2} s^{-1} at a 90% confidence level. The highest peak in the light and spectrum curve indicated the presence of high energy X-ray flares. The fractional variability of 0.444 is relatively high, which indicates that the source is variable. The fall in count per second per energy around 2 keV in the spectrum curve suggests that the intensity of X-rays decreases in a power law manner after a strong flare at this energy. The count-rate distribution of the observation analyzed is best described by a normal distribution which suggests that the emission mechanism in the blazar is governed by additive processes.

Keywords
Blazar Mkn 421, light curve, (log-par+bbody), spectrum, X-ray flares.

Article information
Manuscript received: March 14,, 2023; Accepted: March 31, 2023
DOI https://doi.org/10.3126/bibechana.v20i1.53233

1 Introduction

Blazar Mkn 421, also known as Mrk 421, is a specific blazar and a type of active galactic nucleus (AGN) characterized by high-energy emission from a compact central region. This emission is produced by a jet of matter moving at nearly the speed of light, which is aimed directly at the observer [1]. It is located at 11h04m27.2s and +38012'32"in right ascension and declination, and is one of the closest and brightest blazars with a redshift of z = 0.0308 [2]. The blazar Mkn 421 was one of the first extragalactic sources detected at TeV energies and is one of the brightest BL Lac objects, particularly in the X-ray band [3]. Mkn 421 is believed to be a source of high-energy cosmic rays (CRs) and high-energy neutrinos (HENs) and has strong EM flux and spectral variability [4]. High energy CRs

are the most energetic cosmic rays, with energies exceeding 1018 eV [4]. They are thought to originate from the most extreme environments in the universe, such as supernovae, gamma-ray bursts, or active galactic nuclei (AGNs) like Mkn 421 [5]. Mkn 421 has been extensively studied across the electromagnetic spectrum and is a popular target for multi-wavelength observations. This blazar is a powerful source of high-energy gamma-rays and is one of the first blazars to be detected in this energy range [6]. HENs are subatomic particles with extremely high energies, and they are thought to be produced in the interactions of high energy CRs with matter [7]. The detection of HENs can provide valuable information about the origin and propagation of High energy CRs, and their study can help us understand the most extreme processes in the universe.

The electromagnetic (EM) emission mechanism in Mkn 421, as well as in other blazars, is thought to involve the acceleration and collision of high-energy particles in the relativistic jet. All blazars show variability in their flux and spectrum across the EM spectrum, and emit jets towards Earth [1]. In the case of Mkn 421, it is believed that the relativistic electrons in the jet are accelerated to extremely high energies through various mechanisms, such as shock acceleration, magnetic reconnection, or turbulence [8]. These high-energy electrons then emit EM radiation through various processes, such as synchrotron emission and inverse Compton scattering.

The study of X-rays can provide valuable information about the high-energy particles in the relativistic jet of blazars, such as their distribution and spectrum which is characterized by broad double peaked structure [9]. This structure is obtained in the logarithmic plot of versus . This information can help us constrain the mechanisms responsible for the acceleration of these particles and to better understand the conditions required for the production of HENs and CRs. X-rays are a good tracer of the high-energy emission in blazars, and they can be used to study the connection between the gamma-ray and the X-ray emission. This information can help us understand the underlying physical processes involved in the production of HENs and CRs, such as the interactions between the relativistic particles and the magnetic fields in the jet. X-rays can provide information about the physical conditions in the jet, such as the magnetic field strength, the temperature of the emitting plasma, and the density of the relativistic particles. This information can help us understand the conditions that determine the emission of HENs and CRs and the efficiency of their production in blazars. The observations of X-rays can help to recognize the astrophysical sources that can accelerate particles in the PeV range [10].

XMM-Newton data is used to study the release of the X-ray flares from the galactic and extragalactic sources like blazars, supernova remnants etc. [11]. The maximum count rate in a small interval of time that makes a bump in the light curve is due to the stronger X-ray flares [12]. We analyze the X-ray spectrum in the target sources using 'XSPEC'.

A light curve plots the count rate against time, while a spectrum curve plots the count rate against energy. The best fit model we obtain from the spectrum curve analysis gives insight into the physics processes responsible for the production of X-rays in the sources. Yan et al. (2018) studied the X-ray flares of Mkn 421 using 50 observational IDs and found that all of them were best fit with a combination of two models: log-par and blackbody. This result was based on intraday observations and was consistent when different parameters were plotted against time [13]. This study found that most of the observational IDs of Mkn 421 showed similar results with a reduced chi-square nearly equal to one. On the basis of these findings, we have taken observational ID 0658801301 of Mkn 421 to investigate its flares and emission mechanism.

Liu et al. (1994) analyzed the 28-year historical light curve of ON 231 and found periodic behavior with peaks and minima in the count rate [14]. Similarly, our study also showed similar behavior with a rise and fall in the count rate and a highest peak (see Fig. 1-2). Vila and Romero (2009) [15] used a leptonic and hadronic model for electromagnetic emission in microquasars GX 339-4 to explain the cause of high-energy neutrino emission during X-ray flares as the effect of relativistic jets of particles. This is based on Einstein's theory of the relativistic increase in mass with velocity. Therefore, we use statistical analysis of X-ray data to understand the possible emission of very high energy neutrinos. We have used both light and spectrum curves for our analysis. In this paper, we focus on the target source Blazar.

1.1 *XMM-Newton* instruments

XMM-Newton is a European X-ray satellite mission with 3 high-performance X-ray telescopes and an optical monitor. It has a large X-ray collecting area and can observe sources continuously for long periods, providing highly sensitive observations within 0.15-15 keV [16]. The *XMM-Newton* telescope is highly sensitive due to its advanced instruments, including the European photon imaging camera (EPIC) with CCD cameras and silicon chips [17]. The EPIC cameras have different readout times, with the PN cameras being faster, and are most efficient in the 0.1-10 keV energy range.

The PN detector mode of the EPIC cameras is preferred due to its long lifetime and low photon pile-up problems. In this study, we use EPIC data to focus on the study of X-ray flares.

1.2 X-ray flares and high energy particles emission mechanism

The phenomenon of X-ray flares, where a large amount of energy is released in a short period of time, has been observed in various sources such as blazars. These flares occur at different frequencies in the electromagnetic spectrum [18] and contribute a small fraction to the diffuse neutrino intensity of very high energy [19]. X-ray flares can be detected by a method which is known as the semi-automatic detection procedure [20]. Blazars are classified into two types, BL Lac objects and optically violently variable quasars [21]. BL Lacs are active galactic nuclei with relativistic jets caught at a small angle to the line of sight [1], while quasars are mostly flat-spectrum radio quasars. Blazars are known for their large and quick variations in flux on timescales shorter than 1 hour [22], which is referred to as intra-day variability [23]. Variations on timescales of days to weeks are called short-term variability, and those on scales of months to the longest are known as long-term variability [24]. It is brightest in the X-ray band with the highest flux recorded 1.2 10-9 erg cm-2 s-1 for the energy range 2-10 keV [25]. The energy dissipation mechanism in blazar jets is still not understood. The spectral energy distribution of blazars shows two bumps, with the low-energy bump believed to be synchrotron radiation of relativistic electrons. The origin of the high-energy bump is still under debate, with various mechanisms proposed including inverse-compton scattering [26], relativistic proton synchrotron radiation [27], and synchrotron radiation of secondary particles from proton-proton interactions [28].

2 Materials and Methodology

In this section, we describe the *XMM-Newton* archival data and data reduction techniques that have been used for our work.

2.1 Data (*XMM-Newton* archival data)

XMM-Newton data which is publicly available was used to study the nature of the source in the X-ray band of the electromagnetic spectrum (EM). XM-Newton observations can be retrieved through the *XMM-Newton* Science Archive (http://nxsa.esac.esa.int/nxsa-web). Observation data files (ODFs) were downloaded from the *XMM-Newton* science archive. *XMM-Newton* science analysis software (SAS) was used to reduce this data. Here, EPIC/pn camera observations were used for our purpose because the sensitivity of EPIC/pn is greater than that of the MOS camera [29].

Here, *XMM-Newton* Analysis was performed for one observation ID which is the brightest source blazar (Target: Mkn 421) . For the source analysis, light and spectrum curve was plotted.

2.2 Data reduction techniques

The *XMM-Newton* data was processed using the Science Analysis Software (SAS) version 1.3 with the latest current calibration files (CCF). The energy range from 0.3 to 10 keV was selected for light curve extraction to ensure better quality and higher accuracy, while excluding absorption and background noise. All EPIC/pn observations were taken in small window mode. The source spectrum was extracted from the imaging data of the European Photon Imaging Camera (EPIC), which was set between 10000 and 12000 with the "pattern==0" flag. The presence of pileup in the source was checked, and light curves were extracted from off-source circular regions to detect high background periods caused by flares.

To avoid the strong photon pile-up effects in the inner source regions, event files were extracted from annular regions centered on the source position. The SAS task epatplot was used to test different circular and annular regions and only single pixel events (PATTERN =0) with a quality-flag of 0 were accepted. For EPIC PN, the event list was created using epproc and for EPIC MOS, emproc was run. A light curve was first generated in the energy range of 0.3-10 keV, and then a cleaned event list was produced using a threshold on the light curve counts. This threshold was used to determine "low background" intervals and create the corresponding Good Time Interval (GTI) file. The standard rate values were 0.4 for EPIC PN and 0.35 for MOS data, but these values may change based on the steady light curve. The GTI file produced by the TABGTIGEN tool was used to exclude event lists with flaring background, producing a filtered event list for scientific purposes. The TABGTIGEN tool was utilized to produce a good time interval file, which is devoid of soft proton flares. The source was visualized using ds9, where the source light curve was extracted from a circle and the coordinates of the source and background light curve were obtained. To correct for factors affecting the detection efficiency, such as vignetting, bad pixels, PSF variations, and quantum efficiency, as well as variations affecting the stability of the detection within the exposure, like dead time and GTIs, the cleaned event file was created. The spectral analysis involved generating a redistribution matrix and an-

cillary file available on the *XMM-Newton* SAS site. Finally, the source and background spectra were generated along with arf and rmf files. The spectra were grouped to ensure a minimum of 20 counts for each spectral channel. The spectral analysis of the data was performed using XSPEC and reduced chi square technique is used for statistical methods. Initially, three different models were tried on the data, which included a power law, a broken power-law and a log-parabolic model. The log-parabolic model showed the best fit for the data, and was therefore selected as the main component of a new model. Additional members were added to further improve the fit, and the best result was found to be a combination of a log-parabolic and a blackbody model. This best-fit model provides insight into the triggering mechanism of flares and confirms that the parameters of the system being observed are consistent with the defined model.

2.3 Data analysis techniques

The analysis of Mkn Blazar (Observation ID 0658801301) involves the use of both spectrum and light curve data. The data collected is of high quality with good time resolution and energy coverage. To study individual brightenings in the light curve, a simple logic is used to identify X-ray flares. The light curve displays time and count rate and allows for the study of single-peaked events. Complex multi-peaked flares are broken down into fundamental events, with the peaked events contributing to X-ray flares. The light curve shows that the blazar source is very active with complicated, non-sinusoidal variations, consisting of both short and long period oscillations. Similarly, the spectrum curve is plotted between energy and count rate. The flares in the spectrum curve are identified visually and modeled with elements equal to the number of flares. The fitting of the model is evaluated by analyzing the distribution of residuals, which should be constant if the flare findings are correct. Bumps in the residuals indicate the presence of flares.

Table 1: Log of the observing campaign.

Revolution	Obs. ID.	Target	Start time (UT)	End time (UT)	Duration	Obs. mode
2837	0658801301	Mkn 421	2015-06-05 23:48:35	2015-06-06 07:51:55	29000	Prime Full Window

Table 2: Spectral analysis results of Blazar Mkn 421, with Observation ID 0658801301, fitted with model (logpar+bbody).

Model Parameter	Model Component	Component	Parameter	Unit	Value
1	1	logpar	alpha		2.34 +/- 1.55× 10^{-3}
2	1	logpar	beta		0.22 +/- 4.36 × 10^{-3}
3	1	logpar	pivotE(scale)		1.50
4	1	logpar	norm		6.0 × 10^{-2}+/- 1.55 × 10^{-4}
5	2	bbody	kT	keV	0.6 +/- 5.5 × 10^{-3}
6	2	bbody	norm		5.1 × 10^{-4} +/- 1.11 × 10^{-5}

The variability of a source in *XMM-Newton* observations indicates that the brightness of the source is changing over time. The variability can be caused by various physical processes such as flares and changes in accretion rate onto a compact object like a black hole. The study of the variability of X-ray sources can provide important information about the physical conditions in the source and help to distinguish between different models or theories [30].

Thus to observe variability in source, we find fractional variability which is given in Eq. 1.

$$f_{Vr} = \sqrt{s^2 - < \sigma^2_{err} >} / < x > \qquad (1)$$

where s^2 is the total measured variance, $< \sigma^2 >$ is

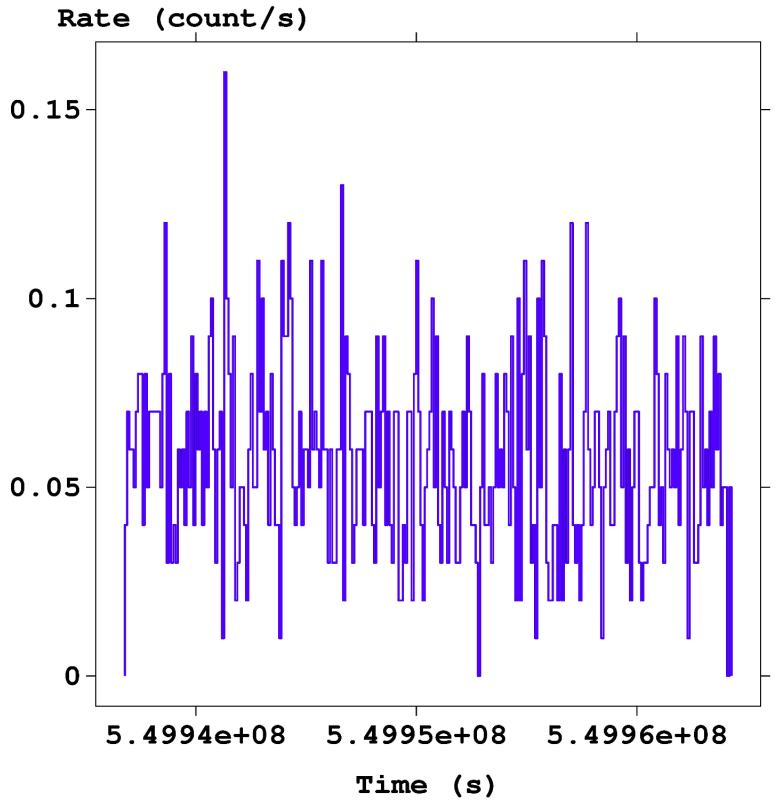

Figure 1: The light curve depicted as a linear-linear axis transformation, displays X-ray flares in a blazar and has been calculated by averaging the data over an 8-hour period ranging from 23:48:35 to 07:51:55.

the mean squared errors, and $< x >$ is the mean count rate [30].

When analyzing the X-ray data, a comparison of the log-normal and normal distributions is made by fitting each to a histogram plot of the count rates per second.

The process of multiple events resulting from the collision of two or more events is referred to as cascade and follows a log normal distribution pattern [31]. Similarly, the normal distribution model is useful for understanding the behavior of X-ray events that are generated through the summing or combining of individual events, rather than through the cascading or multiplication of events [32].

3 Data Analysis And Results

We use both spectrum and light curves for analysis. The source is found to be located at 11:04:29.2118 and +38:12:36.775 of right ascension and declination respectively. The physical coordinate of the source is (25880.5, 27960.5).

3.1 Light curve analysis

The light curve is a plot between count rate and time. The light curve is shown in Figure 1. In the light curve, we have plotted linear-linear axes transformation.

The minimum and maximum time coordinates along the horizontal x-axis are 549935463.28 and 549965603.28 respectively. The maximum count rate coordinates along the vertical y-axis is 0.168 respectively.

In Figure 1, the reference line is set at 0.05. When viewed from 0.05 downwards, the first peak is found at a count rate of 0.04, followed by a second peak with a count rate of 0.034 and a third peak with a count rate of 0.03. There are also fourth

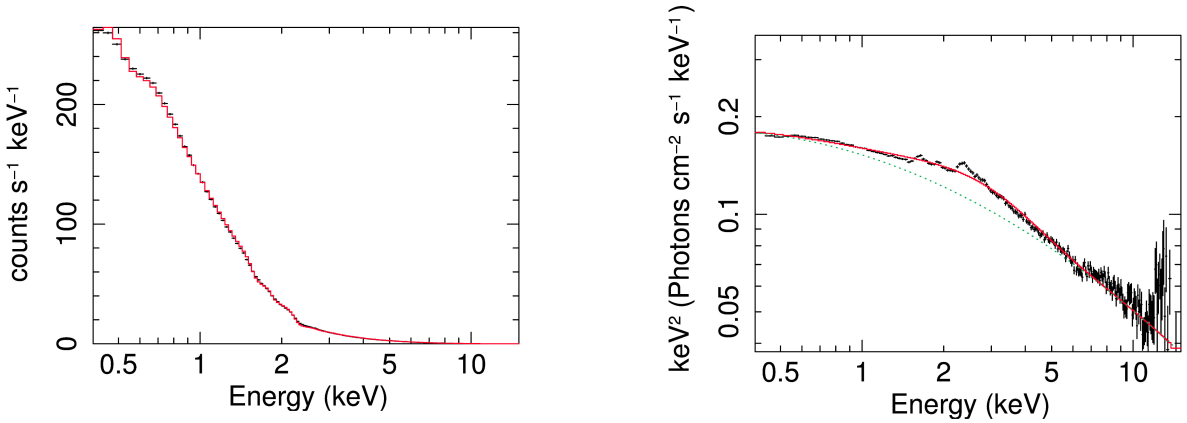

(a) (b)

Figure 2: (a) Left panel: Mkn 421 PN spectrum curve for Observation ID: 0658801301. The observation was performed in imaging mode. The spectrum was fitted with a (logpar + bbody) model. Xdata min = 0.421, Xdata max = 14.40. Ydata min = 1.08 × 10^{-3}, Ydata max = 261.9. Ymodel min = 1.11 ×10^{-3}, Ymodel max = 264.3. (b) Right panel: Unfolded spectrum for the Observation ID: 0658801301. It is well described by a log-parabola (smooth red curve) + blackbody (dashed green) emission model, suffering line-of-sight. absorption.

and fifth peaks with count rates of 0.026 and 0.024, respectively, and a sixth peak with a count rate of 0.019. In Figure 1, when viewed upwards from 0.05, different coordinates (count rates) are observed for each peak, suggesting that the emission of X-rays in Blazar is not periodic over the 8-hour observation period, indicating non-periodic intraday variability. The highest count rate above 0.15 is only observed once in the 8-hour time duration, reflecting the occasional release of relativistic jets in blazar. The highest count rate is associated with high energy, indicating a short and intense energy release.

3.2 Spectrum analysis (for Blazar)

Net count rate (cts/s) for Spectrum is 2.813× 10^2 +/- 1.211 × 10-^{1}(99.9% total). 1-220 channels are noticed. Exposure Time is 1.927 × 10^4sec. Background Exposure Time is 1.927 × 10^4 sec. 7 channels (1-7) were ignored in the spectrum. The attributes or parameters we define in a model describe the properties of the X-ray flares emission mechanism. For example represents the galactic hydrogen column density which is 10^{22} cm^{-2} and set as default in software. 'kT' is the blackbody temperature. Alpha (is the spectral index and beta (is the curvature parameter of the log parabola. Alpha (indicates the slope of the pivot energy. The value of alpha is set as 1.0. The value of beta varies from -4 to +4. But we have set it here as 0.45. The value of pivot energy is set as 1.5. The value of norm (normalization of the model) is set as 1.0. Each parameter has values in a defined range but we have fixed it here so that it fits our model. The best-fitting results exhibit that there is a strong relationship between the parameters we defined.

In the spectral analysis, XSPEC was used. χ^2 statistics were applied during the spectral fittings process Using XSPEC, the X-ray flares can be identified in the spectrum curve plotted between energy and counts per second per energy.

The value of chi-squared is 1377.78 using 213 bins and null-hypothesis probability of 0.001 with 208 degrees of freedom. The value of reduced chi-square (χ^2) = 6.624 (1377.78/208).

The XSPEC analysis of the X-ray data from the observed source yielded a measured integrated flux of 5.015 × 10^{-10} ergs $cm^{-2}s^{-1}$in the energy range of 0.3-2 keV. The associated uncertainty range for this measurement is (5.010 - 5.020) × 10^{-10} ergs $cm^{-2}s^{-1}$, corresponding to a 90% confidence level. In addition, the XSPEC analysis also yielded a measured integrated flux of 2.398 x 10^{-10} ergs $cm^{-2}s^{-1}$ in the energy range of 2-10 keV. The associated uncertainty range for this measurement is (2.392 - 2.405) x 10^{-10} ergs $cm^{-2}s^{-1}$, also corresponding to a 90% confidence level. The best-fitting results for the spectrum curve is shown in Figure 2.

The hard and soft X-ray spectral shapes make the X-ray behavior of blazar very complex. In Figure 2, It is hardened towards lower energies upto around 2 keV and softened towards higher energies (from above 2 keV). The spectrum steepens continuously after around 2 keV. The sharp fall in count rate (intensity) after this particular energy value indicates that brightness decreases after the emission of the flares.

In Figure 1, a light curve is compared to a spectrum curve in Figure 2 to extract properties. The first peak above 0.05 in the vertical y-axis, from the

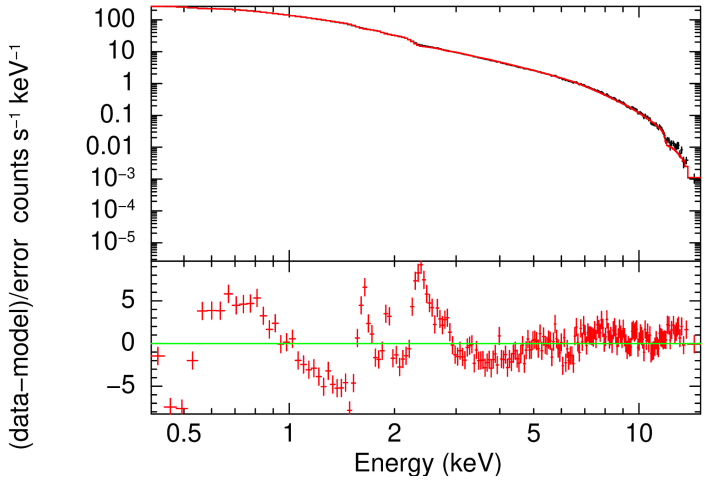

Figure 3: Figure 3: The time-averaged broadband spectrum of the blazar source obtained using *XMM-Newton's* EPIC data (Observation ID 0658801301). The count spectra and residuals with respect to the best-fit (LP+BB) model are displayed on the left in Figure 3, with the residual values on the y-axis and the fitted values on the x-axis.

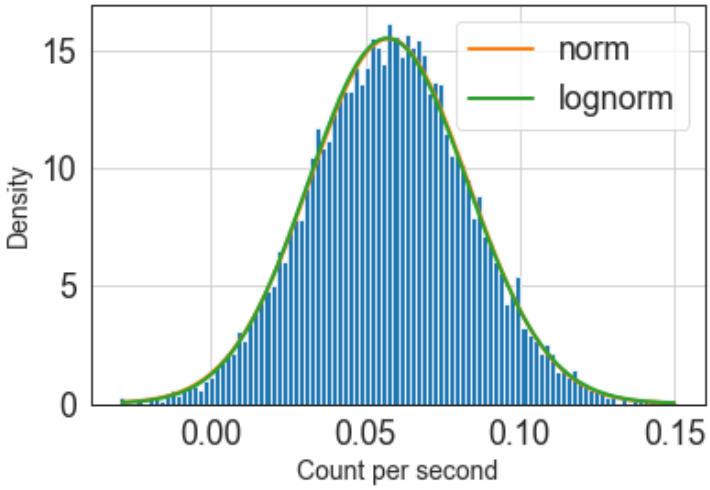

Figure 4: Normal and log-norm distribution of count per second.

reference value 0.05, is referred to as the first lowest peak in Figure 1, while the last peak above 0.15 is referred to as the last highest peak. The number of first lowest peaks, observed from the reference value 0.05, is the greatest in the whole observational period, and the number of last highest peaks is the least, with only one in this case. There are other intermediate peaks in between. When observing Figure 2, it is found that the area under the curve between 0.5 and 1 keV is the maximum and decreases when moving towards the right within the same energy range. By comparing Figure 1 and Figure 2, it is observed that the lowest peak represents the lowest energy and the highest peak represents the highest energy. Higher energy X-rays are emitted in smaller quantities while lower energy X-rays are emitted in greater quantities. The nature of the plot remains the same when different parameters, such as intensity, count rate, residuals, etc., are plotted with respect to either time or energy.

3.3 Counts spectra with residuals

In Figure 3, the count spectra and the residuals are displayed to highlight the patterns in the residuals. The lower panel of Figure 3 showcases the data that deviates from the horizontal line at "0" on the y-axis, which indicates the presence of high-energy X-ray emissions and flare events. The residuals are calculated by dividing the difference between the data and model by the error.

The scatter points in the plot demonstrate that there is non-periodic variability in the count rate per energy in the blazar, which may indicate that the randomness in the count rate per energy is re-

sponsible for producing high energy events.

3.4 Distribution plot analysis

The mean and standard deviation of the count per second are 0.06 and 0.03 respectively. We have tried possible distributions to fit the data such as norm, lognorm and chi2. But the best fit distribution is the normal distribution and represents the additive model which can be interpreted as an addition of events in X-ray observation data analysis. The Kolmogorov-Smirnov (KS) p-value of normal distribution is 0.90. This high KS p-value indicates that the fit is good. Count rate 0.05 appears frequently. The count per second with maximum value 0.16 is only one. This maximum value of count rate appeared only one time during the 8 hour observational period and can be a sign of X-ray flares. The fractional variability is 0.444. A fractional variability value of 0.444 indicates that the variability of the X-ray count rate is 44.4% of the mean squared count rate. This means that there is a significant amount of variability in the X-ray count rate of the source, and that the fluctuations are not due solely to Poisson noise. This value can be used to study the variability of X-ray sources. '0.444' Fractional variability above the Poisson noise level is indicative of physical processes in the X-ray source, such as intrinsic variability, propagation effects, intermittent variability, and correlated variability. Fluctuations in the X-ray emitting regions, such as changes in the accretion rate, can lead to intrinsic variability in the X-ray count rate. Propagation of X-rays through the interstellar medium can lead to additional variability in the count rate due to absorption and scattering. The X-ray source may switch on and off or show variability on different time scales, leading to additional variability in the count rate. Variability in the X-ray source may be correlated with other physical processes, such as variability in the mass accretion rate, leading to additional variability in the count rate. For normal distribution fitting, AIC (Akaike Information Criterion) and BIC (Bayesian Information Criterion) are -107.57 and -55416.87 respectively and for lognormal distribution fitting the AIC and BIC value are -105.76 and -55140.08 respectively.This demonstrates that a normal distribution model is a better fit compared to a lognormal distribution model and indicates that X-ray events are generated by the aggregation of separate events, rather than through a multiplicative progression of events.

4 Conclusion

The X-ray flares in Blazars can be analyzed through a double-component model that consists of the sum of log-parabola and blackbody models (logpar+bb). This model provides a good fit to the 0.3-10 keV emission data with a result of reduced chi-squared ($\chi^2 = 6.624$, and the estimated parameters include an absorbing column density of $= 10^{22}$ cm^{-2}, blackbody temperature of kT = 0.5 keV, pivot energy of 1.5 keV, spectral index of 1.0, and curvature parameter of the log-parabola of 0.45. The parameters of the blazar flare that was studied have been well-constrained and its X-ray variability shows a non-periodic nature in intraday. After the emission of strong flares, the X-ray flux decreases rapidly and steepens downward, especially after reaching a peak value around 2 keV. The non-periodic variability in the count per second may lead to the production of strong flares, which may be associated with emission of high energy neutrinos. The light curve of the blazar source shows signs of bursts, which could be indicative of the production of neutrinos. The best fit normal distribution model indicates that X-ray events result from the additive contribution of physics processes, rather than from the multiplicative cascading.

References

[1] C. Megan Urry and Paolo Padovani. Unified schemes for radio-loud active galactic nuclei. *Publications of the Astronomical Society of the Pacific*, 107(715):803–845, 1995.

[2] M. H. Ulrich, T. D. Kinman, C. R. Lynds, G. H. Rieke, and R. D. Ekers. Nonthermal continuum radiation in three elliptical galaxies. *The Astrophysical Journal*, 198:261–266, 1975.

[3] M. Punch, C. W. Akerlof, M. F. Cawley, M. Chantell, D. J. Fegan, S. Fennell, et al. Detection of tev photons from the active galaxy markarian 421. *Nature*, 358(6386):477–478, 1992.

[4] L. Maraschi, G. Fossati, F. Tavecchio, L. Chiappetti, A. Celotti, G. Ghisellini, et al. Simultaneous x-ray and tev observations of a rapid flare from markarian 421. *The Astrophysical Journal*, 526(2):L81, 1999.

[5] D. Lin, N. A. Webb, and D. Barret. Classification of x-ray sources in the xmm-newton serendipitous source catalog. *The Astrophysical Journal*, 756(1):27, 2012.

[6] D. Yan, S. Yang, P. Zhang, B. Dai, J. Wang, and L. Zhang. Statistical analysis on xmm-newton x-ray flares of mrk 421: distributions of peak flux and flaring time duration. *The Astrophysical Journal*, 864(2):164, 2018.

[7] F. A. Aharonian, M. V. Barkov, and D. Khangulyan. Scenarios for ultrafast

gamma-ray variability in agn. *The Astrophysical Journal*, 841(1):61, 2017.

[8] F. A. Aharonian, M. V. Barkov, and D. Khangulyan. Scenarios for ultrafast gamma-ray variability in agn. *The Astrophysical Journal*, 841(1):61, 2017.

[9] G. Ghisellini, M. Villata, C. M. Raiteri, S. Bosio, G. De Francesco, G. Latini, and M. Mignoli. Optical-iue observations of the gamma-ray loud bl lacertae object s5 0716+714: Data and interpretation. *arXiv preprint astro-ph/9706254*, 1997.

[10] S. Gao, A. Fedynitch, W. Winter, and M. Pohl. Modelling the coincident observation of a high-energy neutrino and a bright blazar flare. *Nature Astronomy*, 3(1):88–92, 2019.

[11] D. Lin, N. A. Webb, and D. Barret. Classification of x-ray sources in the xmm-newton serendipitous source catalog. *The Astrophysical Journal*, 756(1):27, 2012.

[12] J. A. Nousek, C. Kouveliotou, D. Grupe, K. L. Page, J. Granot, E. Ramirez-Ruiz, and et al. Evidence for a canonical gamma-ray burst afterglow light curve in the swift xrt data. *The Astrophysical Journal*, 642(1):389, 2006.

[13] D. Yan, S. Yang, P. Zhang, B. Dai, J. Wang, and L. Zhang. Statistical analysis on xmm-newton x-ray flares of mrk 421: distributions of peak flux and flaring time duration. *The Astrophysical Journal*, 864(2):164, 2018.

[14] F. K. Liu, G. Z. Xie, and J. M. Bai. A historical light curve of on 231 and its periodic analysis. *Astronomy and Astrophysics*, 295:1–10, 1995.

[15] G. S. Vila and G. E. Romero. Leptonic/hadronic models for electromagnetic emission in microquasars: the case of gx 339-4. *Monthly Notices of the Royal Astronomical Society*, 403(3):1457–1468, 2010.

[16] D. H. Lumb, F. A. Jansen, and N. Schartel. X-ray multi-mirror mission (xmm-newton) observatory. *Optical Engineering*, 51(1):011009, 2012.

[17] L. Strueder, N. Meidinger, E. Pfeffermann, R. Hartmann, H. W. Braeuninger, C. Reppin, and H. Soltau. X-ray pn-ccds on the xmm newton observatory. In *X-Ray Optics, Instruments, and Missions III*, volume 4012, pages 342–352, 2000.

[18] D. Garcia Alvarez. Modelling of flares on late-type stars. *Irish Astronomical Journal*, 27, 2000.

[19] K. Murase, F. Oikonomou, and M. Petropoulou. Blazar flares as an origin of high-energy cosmic neutrinos? *The Astrophysical Journal*, 865(2):124, 2018.

[20] M. Gryciuk, M. Siarkowski, J. Sylwester, S. Gburek, P. Podgorski, A. Kepa, and T. Mrozek. Flare characteristics from x-ray light curves. *Solar Physics*, 292(6):1–19, 2017.

[21] X. Rodrigues, A. Fedynitch, S. Gao, D. Boncioli, and W. Winter. Neutrinos and ultra-high-energy cosmic-ray nuclei from blazars. *The Astrophysical Journal*, 854(1):54, 2018.

[22] L. Maraschi, G. Fossati, F. Tavecchio, L. Chiappetti, A. Celotti, G. Ghisellini, and et al. Simultaneous x-ray and tev observations of a rapid flare from markarian 421. *The Astrophysical Journal*, 526(2):L81, 1999.

[23] S. J. Wagner and A. Witzel. Intraday variability in quasars and bl lac objects. *Annual Review of Astronomy and Astrophysics*, 33:163–198, 1995.

[24] A. C. Gupta, D. P. K. Banerjee, N. M. Ashok, and U. C. Joshi. Near infrared intraday variability of mrk 421. *Astronomy & Astrophysics*, 422(2):505–508, 2004.

[25] G. Fossati, A. Celotti, M. Chiaberge, Y. H. Zhang, L. Chiappetti, G. Ghisellini, F. Haardt, A. Pian, G. Tagliaferri, A. Treves, and G. Tavecchio. X-ray emission of markarian 421: New clues from its spectral evolution. ii. spectral analysis and physical constraints. *The Astrophysical Journal*, 541(1):166–181, 2000.

[26] K. Mannheim and P. L. Biermann. Gamma-ray flaring of 3c 279-a proton-initiated cascade in the jet? *Astronomy and Astrophysics*, 253:L21–L24, 1992.

[27] A. Mücke and R. J. Protheroe. A proton synchrotron blazar model for flaring in markarian 501. *Astroparticle Physics*, 15(1):121–136, 2001.

[28] L. Strüder and et al. The european photon imaging camera on xmm-newton: The pn-ccd camera. *Astr. Astrophys.*, 365:L18, 2001.

[29] M. H. Ulrich, L. Maraschi, and C. M. Urry. Variability of active galactic nuclei. *Annual Review of Astronomy and Astrophysics*, 35(1):445–502, 1997.

[30] M. H. Ulrich, L. Maraschi, and C. M. Urry. Variability of active galactic nuclei. *Annual Review of Astronomy and Astrophysics*, 35(1):445–502, 1997.

[31] P. Kushwaha, S. Chandra, R. Misra, S. Sahayanathan, K. P. Singh, and K. S. Baliyan. Evidence for two lognormal states in multi-wavelength flux variation of fsrq pks 1510-089. *The Astrophysical Journal Letters*, 822(1):L13, 2016.

[32] M. Chernyakova, A. Neronov, A. Lutovinov, J. Rodriguez, and S. Johnston. XMM–Newton observations of PSR B1259 63 near the 2004 periastron passage. *Monthly Notices of the Royal Astronomical Society*, 367(3):1201–1208, 2006.